ELSEVIER

Catalysis Today 54 (1999) 143–157

CATALYSIS TODAY

www.elsevier.com/locate/cattod

Towards a precise assessment of the performance of supported photocatalysts for water detoxification processes

Roberto L. Pozzo, Miguel A. Baltanás, Alberto E. Cassano *

INTEC, Instituto de Desarrollo Tecnológico para la Industria Química, Universidad Nacional del Litoral and Consejo Nacional de Investigaciones Científicas y Técnicas, Güemes 3450, 3000 Santa Fe, Argentina

Abstract

The performance of Degussa P-25 titanium dioxide photocatalyst in a water environment and two different forms of operation was studied. The finely divided powder was used in a suspended bed (slurry) reactor, and the same catalyst was physically supported on quartz sand and employed in a fluidized bed reactor. Both reacting systems were operated under conditions of a fully irradiated photoreaction space (FIP reactor) and the comparison was made for the same mass concentration of catalyst per unit reactor volume (250 ppm) using different combinations of bed expansion and surface coverage of the support. A tubular black light lamp was placed inside an annular reactor, where the photocatalytic oxidation of a model compound (oxalic acid) was investigated.

Results were analyzed in terms of initial reaction rates per unit reactor volume and per unit of the liquid phase volume inside the reactor. Likewise, apparent quantum efficiencies were evaluated for the initial conditions, using the concept of apparent captured radiation power. It was found that the efficiency of the slurried photocatalyst is approximately five times larger than in the supported form. Among the different fluidized bed operations the highly expanded bed, with 100% coverage of the support surface, was found to be the most convenient condition for the immobilized titania.

Keywords: Supported photocatalysts; Fluidized bed; Reactor performance; Apparent quantum efficiencies

1. Introduction

Degradation of organic pollutants in water and air by heterogeneous photocatalysis has been increasingly investigated as a viable alternative in the last two decades [1–4]. This approach is based on the possibility of handling near UV radiation to excite a semiconductor (usually titanium dioxide). Electron-hole pairs photogenerated in the semiconductor solid particles originate a redox environment. The formation of extremely reactive $OH^{\bullet}$ radicals from water [5] and *direct* oxidation of the pollutant species by hole trapping [6] have been postulated as the most likely main reaction mechanisms. However, sustaining the charge balance, electrons can reduce adsorbed oxygen at the semiconductor interface thus generating other intermediate species of high oxidation properties.

In principle, photocatalysts can be employed either as finely divided powders suspended (slurried) in the aqueous media or immobilized on a suitable support material (e.g., quartz sand, glass, silica gel, optical fibers, alumina clays, ceramics), operating in either fixed or fluidized bed configurations. From an engineering point of view the second alternative is

* Corresponding author. Tel.: +54-342-4559175; fax: +54-342-4550944

E-mail address: acassano@arcride.edu.ar (A.E. Cassano)

0920-5861/99/$ – see front matter
PII: S0920-5861(99)00176-5

preferable, so as to avoid costly particle-fluid separation stages downstream. Also, because of the small particle size of the catalyst powders usually synthesized by the industry (somewhere between 30 and 300 nm in diameter), the operating costs of this downstream operation may become prohibitive, thus invalidating the energy saving of these decontaminating processes altogether.

On the other hand, though, the efficiency of slurry-type photocatalytic reactors has been claimed to be higher than the one achievable with immobilized photocatalysts [7]. Nevertheless, given the complexity of the photocalytic process and the multiplicity of variables involved, it is not an easy task to find a common ground for performance comparisons. The penetration length of light in the solid–liquid medium is, of course, one of the significant parameters to be taken into account. It depends, among other variables, on particle size, catalyst loading (slurry concentration in one case, support surface coverage and support bed density in the other) and support transparency to radiation. But, also, in order to clarify the efficiency issue it is of outmost interest to be able to compare the performance of the same catalyst type under different reactor configurations.

With this goal in mind, special attention was given in this work to ensure similar basis for irradiation and catalyst loading in the illuminated volume, using a single photocatalyst with identical structure and texture (Degussa P-25 titania) to make comparisons between the performance of its slurried, powdery form and that resulting from its use in fluidized beds, after its fixation onto an inert support. A broad set of conditions for bed expansion, catalyst loading and/or percentage of surface coating were used.

In general, catalyst fixation can be carried out either by in-situ catalyst generation (i.e., sol-gel process, chemical vapor deposition, grafting) or by manipulation of previously made titania powder (PMTP) [7]. For the indicated reasons the last alternative was chosen in this work, since it allows to contrast the performances of the same catalyst both as a free powder and immobilized.

Quartz sand was employed as the supporting material because it is fairly transparent to near UV radiation, has an acceptable surface bonding capacity with TiO_2 and provides a physical configuration that favors an easy liquid–solid separation. Its use in a fluidized bed facilitates reactor designs-of the type used in the present work-where normally there are no mass and heat transfer limitations.

Oxalic acid has been taken as a convenient model reactant since it is non volatile, is easy to analyze and readily decomposes without intermediates, to give carbon dioxide:

$$C_2O_2(OH)_2 + \tfrac{1}{2}O_2 \Rightarrow 2CO_2 + H_2O \quad (1)$$

with an apparent zero-order reaction rate under well defined operating conditions [8,9], which is particularly advantageous.

2. General approach

One of the main pre-requisites to provide a meaningful comparison of performances among different catalyst configurations in terms of specific reaction rates is to have a very well defined irradiated volume. Accordingly, the fully irradiated photoreactor concept, or FIP reactor [10] (i.e., where photons are always available inside the whole reactor volume), was adopted to perform the experimental work. Hence, both the reactor dimensions and the catalyst concentrations, were carefully chosen in each case so that always a remnant flux of energy leaving the reaction volume could be detected after the light has gone through it.

From an engineering point of view, a meaningful performance evaluation should additionally take into account the fraction of solid volume present in the reactor volume (ϕ_s), which is particularly significant in the fluidized bed configurations. From this optic, if one focused on the energy spent on liquid recirculation, the net-liquid volume fraction in the reacting annulus ($\phi_L = 1 - \phi_s$) would be the relevant normalizing parameter to establish a comparison yardstick. However, if radiation energy were the cost-determining factor, the interest would be centered in optimizing the utilization of the total illuminated reacting volume. In such a case, this total volume would be the appropriate reference to be used for reaction rates and catalyst concentration settings. In this work the experimental results are then analyzed from both perspectives.

Also, in order to compute and compare efficiencies one of the key problems is the correct evaluation of the absorbed radiation inside the heterogeneous reactor. In principle, this evaluation can be carried out by apply-

ing the radiative transport equation to the participating system [11,12] but, in these heterogeneous media absorption and scattering effects are combined, and the radiative transfer equation has an integro-differential nature. Moreover, the relevant properties required to solve this equation (i.e., the absorption and scattering coefficients) are very difficult to measure.

An evaluation of these optical parameters for different brands of powdered titania in aqueous suspension was recently published by Cabrera et al. [13]. However, there are not equivalent published data relative to fixed titania either on sand or on other supports. (An experimental program aimed at evaluating these optical parameters in fluidized beds is currently in progress in this laboratory).

Alternatively, and only for comparison purposes, in the present work an *apparent captured power* (P_C) is defined in terms of the illuminating incident power onto the reacting space (P_{IN}) and of the remaining power leaving the reaction space after the interaction has occurred (P_{OUT}). The character of '*apparent*' specifically refers to (P_{IN}), since not all the incident power effectively enters into the reaction volume, due to the (surely significant) back scattering phenomenon.

With the same objective apparent quantum efficiencies have also been defined, in terms of the ratios of the initial rates of decomposition of oxalic acid per unit volume of reactor and of the liquid phase inside the reactor versus the corresponding captured power by the reacting volume.

3. Experimental work

3.1. Experimental set-up.

Fig. 1 shows a schematic flow sheet of the experimental set up. The main features and dimensions of the device, which essentially consisted of a multitube annular photoreactor with three annular spaces, are detailed in Table 1. A tubular black light lamp (Philips TLD 18W/08; nominal output power: 18 W; superficial emission from 300 to 400 nm, with a peak at 350 nm) was centered at the photoreactor axis. Its operation (intensity, voltage and input power) was continuously monitored, and previsions were taken to ensure the proper operation of the lamp according to its nominal power. Besides, the lamp was used after a minimum of 100 h of monitored operation to make sure that it was working within the most stable period of its average lifetime. Recycling systems were driven by variable speed peristaltic pumps (Masterflex, Model 2650 MG. The temperature was kept constant (295 K) using a thermostatic bath (MGW Lauda K4R).

The photoreactor itself consisted of a set of four Pyrex glass tubes constituting three coaxial annuli (Fig. 2). The interior annulus was used as a thermostat. The central annulus allowed, first, the actinometric measurement of the incident radiation at the reaction space, and served later as the main reaction vessel. The outer annulus was an actinometric space where the exiting radiation, outgoing from the reaction vessel, was evaluated. By this way, satisfaction of FIP conditions (i.e., all the particles along the light path can see the photons) could be monitored.

3.2. Materials and methods

A model titania photocatalyst: (Degussa P-25, ~75% anatase; $S_g \cong 50\,m^2\,g^{-1}$; $d_p = 30$–70 nm), a model support: (Aldrich quartz white sand, Cat. No. 27,473-9; $r = 2.4\,g\,cm^{-3}$; particle size: +50/−70 mesh) and a standard aqueous solution of a model reactant: $5 \times 10^{-7}\,mol\,cm^{-3}$ oxalic acid di-hydrate (Carlo Erba RSE, 99.9%), were used throughout the work. In all cases the titania photocatalyst was dried at 120°C for 12 h before it was used. Water was 'ultrapure', i.e.: triply distilled, demineralized, free of organic content and filtered (0.2 μm membrane).

Immobilization of the TiO_2 powder on quartz sand was carried out as follows: a fraction of the 'as received' sand, of particle size +50/−60 mesh (210–240 μm) was selected as the supporting material by screening, and washed in acetone to remove organic matter. Calculated amounts of TiO_2 powder were thoroughly dry-mixed with approximately 400 g of the supporting material in a rotavapor of 1000 cm^3 capacity for about 12 h. The mixture was then gradually humidified (drop by drop) with approximately 300 cm^3 of water until consistency of a fluid 'paste' was observed and therewith evaporated until complete dryness under vacuum-controlled conditions in the same rotavapor. The desiccating temperature, (around 370 K) was gradually reached with a temporal step of about 1°C/min. Finally, the TiO_2 coated sand (CS) was immediately calcined in a oven at 673 K for 12 h. This

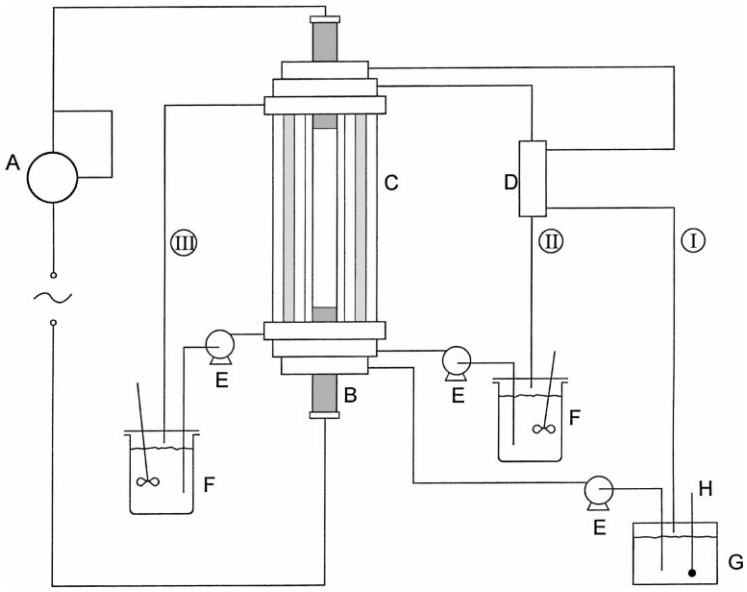

Fig. 1. Experimental set-up: (A) watt-meter, (B) lamp, (C) photoreactor, (D) heat exchanger, (E) peristaltic pump, (F) reservoir, (G) thermostatic bath, (H) thermometer, (I) refrigeration loop, (II) reaction loop, (III) actinometric loop.

Table 1
Lamp and reactor characteristics

Device	Annulus	Parameter	Value	Units
Lamp		nominal power	18	W
		diameter	2.6	cm
Black light		total length	60.0	cm
Philips TLD 18W/08		unmasked length	23.5	cm
Reactor	1 (temperature control)	internal radius	2.25	cm
		external radius	3.00	cm
Concentric cylindrical tubes made of pyrex glass		length	44.1	cm
		volume	546.0	cm^3
	2 (reaction space)	internal radius	3.25	cm
		external radius	4.00	cm
		length	36.0	cm
		volume	615.0	cm^3
		cross section	17.1	cm^2
	3 (actinometer space)	internal radius	4.50	cm
		external radius	5.30	cm
		length	30.0	cm
		volume	739.0	cm^3
		cross section	24.6	cm^2

fixation-calcining method was able to ensure excellent mechanical stability of the coating for at least 12 h of continuous operation in liquid solid fluidized beds.

Three nominal degrees of sand coverage with TiO_2 were programmed: one monolayer (corresponding to about 1 mg of TiO_2/g sand), 60 and 40% of a monolayer, respectively. The amounts of photocatalyst actually deposited were evaluated by UV-spectroscopy (410 nm), after previous digestion of aliquots of the three batches of coated sand with $(NH_4)_2SO_4$ [14].

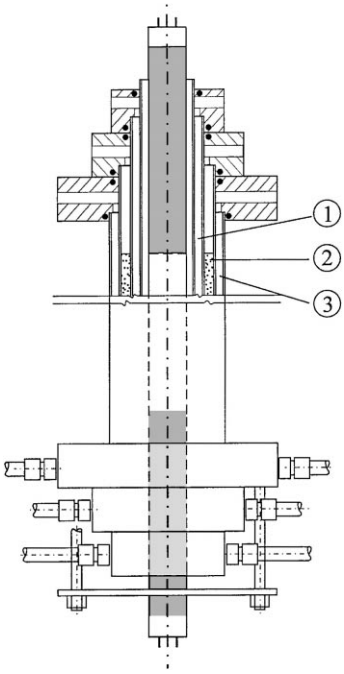

Fig. 2. Multitube annular photoreactor: (1) temperature control space, (2) reaction space, (3) actinometer space.

The batches of CS were found to contain 1.16, 0.64 and 0.34 mg of TiO_2/g of sand, respectively.

As indicated in Section 1, our experimental program was aimed at comparing the performance of the same photocatalyst (Degussa P-25) in both its suspended and immobilized form, under carefully controlled conditions and using a fully illuminated photoreactor.

So, to make certain that the immobilization treatment would not alter the properties of titania, samples of dry ('as is'), calcined (673 K, 12 h) and wetted, then calcined P-25 were compared. By X-ray diffraction it was verified that after these calcining treatments the degree of crystallinity of the TiO_2 did not change and that the anatase to rutile ratio was preserved as well.

A suspension containing 250 ppm TiO_2 was used as the comparison yardstick. The apparent Napierian extintance of this suspension is such that for the radial gap of our photoreactor the FIP conditions are still attainable while, at the same time, the chemical conversion is maximized [10].

Accordingly, to realize a set of experimental conditions under which the same mass of immobilized TiO_2 was used, three degrees of expansion of the fluidized bed (up to the same geometrical level in the reactor) were employed: 7.0-, 3.8- and 2.3-times the unexpended bed volume, respectively. Table 2 contains additional data about these fluidized beds.

Table 2
Fluidized bed operating conditions

	Fluidized bed expansion		
	Low	Medium	High
Nominal expansion	2.3	3.8	7.0
Solid volume fraction ($\phi_s = V_{CS}/V_{FB}$)	0.43	0.26	0.14
Mass of sand in the bed, g	375	198	110
Liquid flow rate, $cm^3\,s^{-1}$	14.6	28.3	40.0
Superficial velocity, $cm\,s^{-1}$	0.82	1.58	2.24
Fluidized bed height, cm	30	30	30
Fluidized bed volume, cm^3	512	512	512

In total, six different combinations of sand coverage and bed expansion were tested. To facilitate future analysis they are shown in Fig. 6, in matrix form, together with the corresponding amounts of catalyst involved. In Fig. 6 the bed expansion increases vertically and, so, the volume fractions of solid (ϕ_s) decreases in the same direction. Surface coverage increases horizontally.

The numbers inside each box of the matrix represent the concentration of catalyst in the reacting volume (mg TiO_2 per unit volume, in ppm):

(a) as the mass of TiO_2 per unit volume of the fluidized bed, $\left[C_{TiO_2}\right]_{V_R}$ (lower row inside each box, boldface), and

(b) as the mass of TiO_2 per unit volume of the liquid phase in the fluidized bed, $\left[C_{TiO_2}\right]_{V_{Liq}}$

As it can be observed in the diagram, the matrix diagonal represent conditions for which the concentration of TiO_2 inside the reaction volume ($[C_{TiO_2}]_{V_R} = 250$ ppm) is the same as the concentration of the suspension of the unsupported catalyst, used for comparison purposes in slurried form. The columns represent conditions for which surface coverage is constant, so that higher bed expansions involve lower catalyst concentrations. The rows indicate the corresponding catalyst concentrations which, of course, are higher the higher the surface coverage is. The three combinations corresponding to the lower right corner of the matrix were not included in the testing program since under these experimental conditions (low bed expansion together with high surface coverage) FIP operation was no longer attainable.

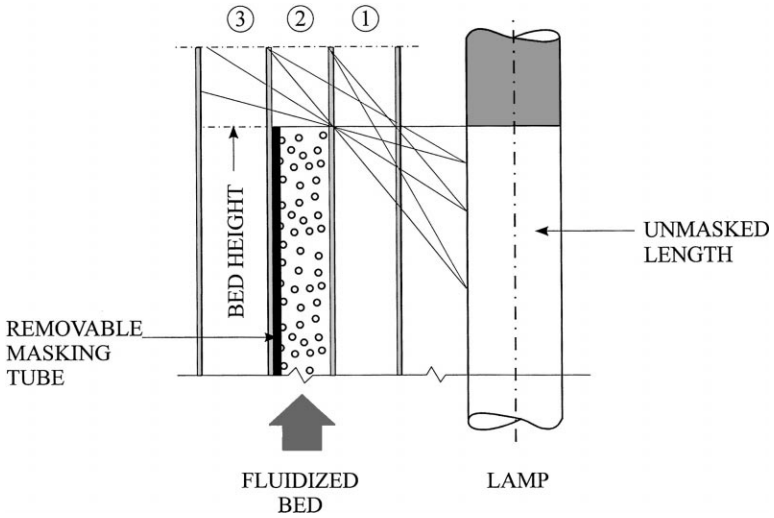

Fig. 3. Partial view of the photoreactor: even for a completely opaque fluidized bed (simulated with a removable masking tube) a portion of the actinometer space can still be reached by radiation emerging from the lamp.

For comparison purposes additional runs were included, aimed at evaluating the captured radiation with 0 coverage (i.e., no TiO_2 added) and for the same bed expansions.

The degradation of oxalic acid was followed by analyzing total organic carbon, with a 5000A Model, TOC SHIMADZU analyzer. Actinometric measurements were carried out with 0.006 M potassium ferrioxalate, by conventional techniques [15].

3.3. Experimental procedure

Steady state temperature and lamp operation conditions were achieved prior to initiating any experimental run, by circulating ultrapure water at constant temperature through the annular Space 1 (Fig. 2) during 2–3 h.

A suitable actinometric solution (potassium ferrioxalate, 6×10^{-6} mol cm^{-3}) was recirculated through the annular Space 3 (Fig. 2). The reservoir V_T^{III} contained 1760 cm^3 of this solution, as well as provisions for sampling and temperature control. The device was used to measure the radiation going out from the reaction space (Space 2), when either the TiO_2 suspension was circulating through it or a fluidized bed of titania immobilized onto the sand was inside the reaction volume.

Since in the last case, the fluidized bed in its different versions was always expanded up to a level equal to the highest limit of the emitting length of the lamp, a fraction equivalent to a 20% of the total volume of the annular Space 2 was empty of radiation extinguishing material (Fig. 3). Consequently, an experimental configuration was implemented to discern the remaining energy leaving the central annulus after interacting with the fluidized bed, from that passing through a bed-free volume fraction. This fraction of outgoing energy power was evaluated by masking the reacting bed space with a cylindrical opaque tube, simulating so a totally 'black' fluidized bed (Fig. 3).

Through the intermediate tube (annular Space 2) were recirculated, alternatively, in the closed Loop II:

(a) The actinometric ferrioxalate solution, which was used to obtain the incident radiation power. In this case the reservoir tank of the loop was filled with $V_T^{II} = 19{,}400$ cm^3 of testing solution, under continuous stirring to ensure sampling homogeneity.

(b) A suspension (250 ppm) of titanium dioxide in an air-saturated solution of oxalic acid (0.5 mM). In this case the volume of solution in the reservoir was $V_T^{II} = 4400$ cm^3, and the suspension was also homogenized, by mechanical agitation.

(c) An air-saturated solution of oxalic acid prepared also with ultrapure water, recirculating through the fluidized beds of titania-coated quartz sand at

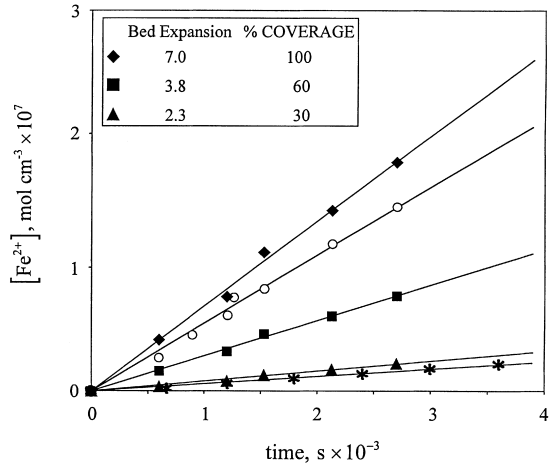

Fig. 4. Actinometer experimental results (outer annular space): The time evolution of $[Fe^{2+}]$ is directly proportional to the outgoing radiation from the reaction space. TiO_2 was used in suspension (slurried) (○) or immobilized onto quartz sand (fluidized bed) (◆, ■, ▲). $[C_{TiO_2}]_{V_R} = 250$ ppm. (*) With a removable mask placed at the outer wall of the reaction space.

appropriate flow rates. The circulation flow rates were chosen to allow stable fluidized bed operation while at the same time the annular Space 2 could be filled up to the predetermined level, with a fluidized bed of CS at the three different bed expansions previously mentioned. For these runs the liquid volume in the reservoir was: $V_T^{II} = 1400$ ml.

4. Results and discussion

4.1. Actinometry

Fig. 4 shows typical actinometric data obtained with the 6 mM potassium ferrioxalate solution circulating through the outer annular space. It shows the linear evolution with time of the concentration of ferrous ion $(C_{Fe^{2+}})$, generated by the radiation going out from the reaction space (annular Space 2), for the titania slurry and for different combinations of bed expansion and surface coverage of TiO_2, respectively.

In this figure, the amount of titania contained inside the annular Space 2, expressed in terms of the $[C_{TiO_2}]_{V_R}$ parameter, was kept constant (250 ppm). Data from an additional run, in which the reacting space was masked with a cylindrical opaque tube to simulate a totally 'black' fluidized bed are shown as well. They certainly indicate that the spherical characteristic of the lamp emission can generate reaction of the actinometer in the outer annulus even when the nominal reactor volume is masked (See Fig. 3).

The FIP operation can be confirmed whenever a net measurable actinometric reaction can still be observed after the corresponding data for the masked annulus have been subtracted. It is apparent from Fig. 4 that for both the slurried catalyst and each of the fluidized beds the FIP condition was achieved. It also emerges that the fluidized bed expansion has a decisive gravitation on radiation extinction: The outgoing radiation from the most expanded bed (7.0) was more than the one from the titania slurry and conversely, the actinometric reaction from the least expanded bed hardly overcame the one pertaining to the reactor-masked condition. The remaining combinations of fluidized bed expansion and surface coverage also satisfied the FIP requirement, since they all correspond to either less surface coverage for the same bed expansion, or higher bed expansion at same coverage of the sand with TiO_2.

These experimental results, obtained by recirculating the actinometer between the outer annulus $\left(V_{R,3}^{Act}\right)$ and the well-mixed external reservoir V_T^{III}, can be easily analyzed by taking advantage of the following design features of the experimental settings: (1) differential per pass conversion of the actinometer inside the reactor was always achieved; (2) the actinometric reactor volume was always smaller than the total volume of the recycling system, and (3) all the energy entering the actinometric reaction volume is absorbed by the actinometer.

Thus, the actinometric reaction always proceeds into a continuous differential reactor inside the loop of a batch recirculating system. So, under steady operating conditions for the lamp and constant temperature, the following relation applies [10]:

$$\frac{dC_{Fe^{2+}}(t)}{dt} = \frac{V_{Act}}{V_T^{III}} \left\langle R_{Fe^{2+}}(\vec{r}) \right\rangle_{V_R^{Act}} \quad (2)$$

For this actinometric reaction, the ferrioxalate decomposition is of first order with respect to the local volumetric rate of energy absorption, e_λ^a and of zero-order with respect to the oxalic acid concentration [15] and so the following equation applies to the local rate:

$$R_{Fe^{2+}}(\vec{r}) = \int_\lambda \Phi_\lambda \, e_\lambda^a(\vec{r}) \, d\lambda \quad (3)$$

However, because the radiation field is not uniform, the observable reaction rate is always a volume-averaged (albeit time-independent) value:

$$\left\langle R_{Fe^{2+}}(\vec{r})\right\rangle_{V_R^{Act}} = \int_\lambda \Phi_\lambda \left\langle e_\lambda^a(\vec{r})\right\rangle_{V_{R,3}^{Act}} d\lambda \quad (4)$$

By integrating Eq. (2) with the initial condition

$$C_{Fe^{2+}} = 0 \quad \text{for} \quad t = 0 \quad (5)$$

$$C_{Fe^{2+}}(t) = \frac{V_{R,3}^{Act}}{V_T^{III}} \left\langle R_{Fe^{2+}}(\vec{r})\right\rangle_{V_{R,3}^{Act}} (t - t_o) \quad (6)$$

that is, linear profiles for $C_{Fe^{2+}}$ versus time are predicted, which is experimentally verified in Fig. 4 for each run.

If for the overlapping wavelength range corresponding to lamp emission and Pyrex glass transmission ($300\,nm \le \lambda \le 400\,nm$) one assumes that the quantum yield of the potassium ferrioxalate reaction has a rather mild dependence with wavelength (which is a very good approximation), one can introduce the following change in Eq. (4):

$$\left\langle R_{Fe^{2+}}(\vec{r})\right\rangle_{V_{R,3}^{Act}} = \langle\Phi_\lambda\rangle_\lambda \int_\lambda \left\langle e_\lambda^a(\vec{r})\right\rangle_{V_{R,3}^{Act}} \quad (7)$$

It is then immediate that Eq. (6) can be rewritten so as to give a direct estimate of the radiation power outgoing from the reaction space, P_{OUT}:

$$P_{OUT} = V_{R,3}^{Act} \int_\lambda \left\langle e_\lambda^a(\vec{r})\right\rangle_{V_{R,3}^{Act}} = \frac{V_T^{III}}{\langle\Phi_\lambda\rangle_\lambda} \frac{C_{Fe^{2+}}(t)}{(t - t_o)} \quad (8)$$

When the central annulus is masked up to the upper level of the fluidized bed to simulate a 'black' fluidized bed into the reaction volume, the measured power in the outer actinometric space corresponds to the radiant energy still crossing through the upper (i.e., free of reacting bed) portion of the central annulus, P_M as already pointed out.

An expression formally identical to Eq. (7) is obtained when the actinometer solution is made to circulate through the reaction Space 2, using the external reservoir V_T^{II} in closed circuit. In this case the calculated value of the radiation power corresponds to the incident radiation onto the reaction space, P_{IN}:

$$P_{IN} = V_{R,2}^{Act} \int_\lambda \left\langle e_\lambda^a(\vec{r})\right\rangle_{V_{R,2}^{Act}} = \frac{V_T^{II}}{\langle\Phi_\lambda\rangle_\lambda} \frac{C_{Fe^{2+}}(t)}{(t - t_o)} \quad (9)$$

For the catalyst slurry, an *Apparent per cent captured power* can be simply defined as:

$$P_C^{Susp}\% = \left(\frac{P_{IN} - P_{OUT}}{P_{IN}}\right) \times 100 \quad (10)$$

In the case of the fluidized bed reactor, however, it should be noticed that by controlling the bed expansion the true reactor volume becomes defined by the height of the reaction space actually occupied by the coated sand. The reactor volume corresponding to the slurry operation, on the other hand, is the total volume of the illuminated central annular space.

Consequently, for the fluidized bed the corresponding expression for the apparent captured power should be modified as follows:

$$P_C^{FB}\% = \left(\frac{P_{IN}\Psi_{FB} - (P_{OUT} - P_M)}{P_{IN}\Psi_{FB}}\right) \times 100 \quad (11)$$

where Ψ_{FB} is a partitional factor which takes into account the actual incident power at the reactor surface that can interact with the reacting medium and it is defined as:

$$\Psi_{FB} = \frac{\text{Incident radiation onto the inner surface of the fluidized bed reactor}}{\text{Incident radiation onto the inner surface of the slurry reactor (Space 2)}} \quad (12)$$

Owing to axial non-uniformity of the lamp emission, though, this correction is not directly proportional to the relative reactor heights [16]. Therefore, to evaluate Ψ_{FB} a three-dimensional radiation emission model was applied to compute the energy power arriving to the reactor wall from the lamp (See Appendix A).

Fig. 7 presents in matrix form the apparent captured power ($P_C\%$) of the fluidized beds used in this work, as a function of bed expansion and surface coverage, including the uncoated sand (0% TiO_2 coverage). The corresponding value of $P_C\%$ for the TiO_2 suspension is also shown.

The data show that the apparent captured power of these fluidized beds is a strong function of bed expansion. This is particularly evident for 0% TiO_2 coverage (first column), with a $P_C\%$ variation of about 70% between the lowest and the highest bed expansion, respectively. The data also indicate that $P_C\%$ is increasingly sensitive to surface coverage, the

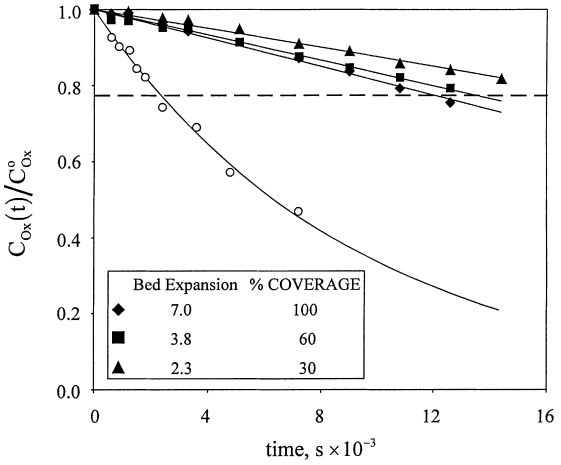

Fig. 5. Oxalic acid concentration (dimensionless; $C^0_{Ox} \cong 5 \times 10^{-7}$ mol cm^{-3}) versus time, using the photocatalyst in suspension (slurried) (○) or immobilized onto quartz sand (fluidized bed) (◆, ■, ▲). $[C_{TiO_2}]_{V_R} = 250$ ppm. The dashed line represents conditions below which the order of reaction is no longer 0 (see text).

higher the bed expansion is. This is observable just by comparing the relative increments of P_C% for 0 and 30% surface coverage at each bed expansion (first and second columns). The increments are: 120, 40 and only 7% for the highest, medium and low expansion, respectively.

Interestingly, the increment of the apparent captured power with surface coverage within the titania coated samples is just moderate. For the highest expansion (first column) this increment is only of about 14% when going from 30 to 100% coverage.

For this annular space the 250 ppm suspension was able to capture a 79.3% of the incoming radiation. As Fig. 7 suggests, this 'capture power' can be matched by suitable combinations of sand coverage and bed expansion. Most important, the apparent capture power of the bare, inert sand is by no means negligible.

4.2. Oxalic acid decomposition

Fig. 5 shows typical experimental data of the time evolution of the oxalic acid decomposition, normalized with the initial concentration ($C^0_{Ox} = 50$ ppm), for three different conditions of surface coverage and expansion of the fluidized bed but carrying the same amount of catalyst inside the reaction volume: $[C_{TiO_2}]_{V_R} = 250 \times 10^{-6}$ g cm^{-3} (250 ppm, matrix diagonal in Fig. 6). The performance of the slurry system using the same catalyst concentration inside the reaction volume is also presented in this figure.

As a first observation it clearly emerges that, for the same catalyst placed into the reaction vessel at the same concentration, the supported material in fluidized bed operation always shows a significant decrease in photocatalytic conversion as compared with that obtained in the dispersed powder (slurry) form. It can be also observed an apparent zero-order reaction with respect to C_{Ox}, in all cases, even for the slurry system, at least up to about 20% conversion.

With this same photocatalyst (Degussa P-25) Herrmann et al. [8] reported also zero-order reaction in the photo oxidation of oxalic acid for substrate concentrations higher than 480 ppm, but using a concentration of 2500 ppm of the TiO_2 slurry. To validate the comparison of their data with ours, where $[C_{TiO_2}]_{V_R} = 70 - 250$ ppm and $C_{Ox} \cong 50$ ppm, a common basis has to be taken. Fortunately, as both data come from slurries of the same Degussa P-25 powder, only the specific initial concentration (i.e., ratioed

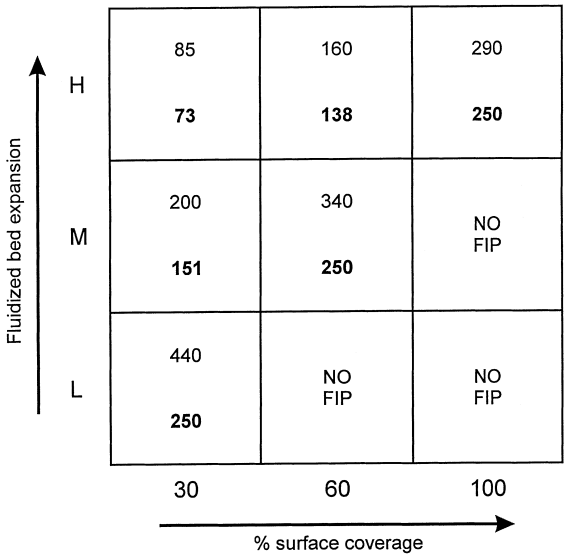

Fig. 6. Fluidized bed operation: concentration of photocatalyst (ppm) inside the reaction annulus, expressed as: the mass of TiO2 per unit volume of the fluidized bed, $[C_{TiO_2}]_{V_R}$ (lower row of each box, boldface), and as the mass of TiO_2 per unit volume of the liquid phase in the fluidized bed, $[C_{TiO_2}]_{V_{Liq}}$ (upper row of each box), for different bed expansions and percentages of surface coverage of the quartz sand.

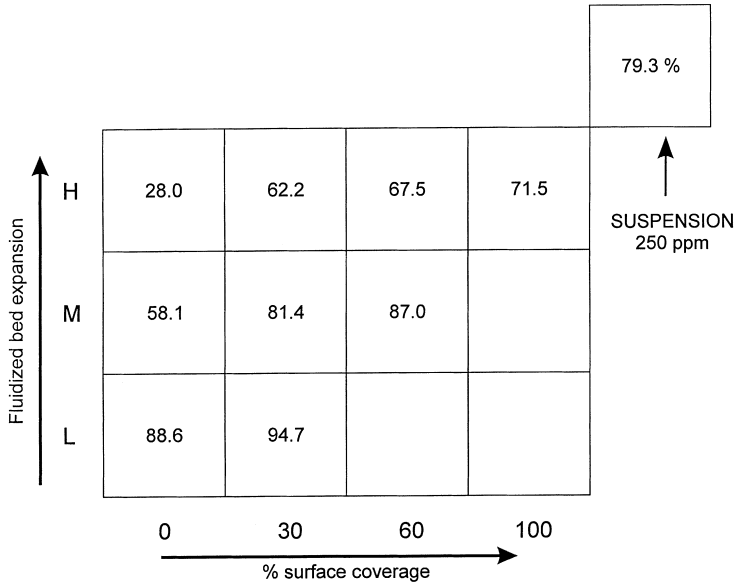

Fig. 7. Apparent captured power inside the reaction space, P_C%, with the TiO_2 used in suspension (250 ppm) or in fluidized bed form, for different bed expansions and percentages of surface coverage of the quartz sand [see Eqs. (10) and (11)]. The apparent captured power of the fluidized beds using the uncoated quartz sand is also included.

with the amount of catalyst present in the system) suffices: $C^0_{Ox}/\left[C_{TiO_2}\right]_{V_R}$. This lower limit ratio gives a value of (480/2500=) 0.19 for Herrmann et al.'s data, which compares very well with the minimum similar ratio (50/250 =) 0.20 used in the present work. Hence, one can surely conclude that in all of our experiments a zero-order reaction rate with respect to oxalic acid concentration should be expected when the conversion is less than about 20%.

The decomposition reaction was conducted under the following process and design conditions: (a) hydrodynamic and thermal steady-state, (b) perfect mixing inside the reservoir (V^{II}_T), (c) negligible volume of the connecting lines, (d) zero reaction rate outside the illuminated reacting volume (V_R or V_{FB}, for the slurry or the fluidized beds, respectively), (e) high recirculating flow rate and (f) ratio of reactor volume to total volume smaller than one. Furthermore, the system was always operated as a continuous differential reactor inside the loop of a batch recirculating system so that the mass balance equation for the organic substrate is quite similar to Eq. (2):

$$\frac{dC_{Ox}(t)}{dt} = -\frac{V_R}{V^{II}_T}\langle R_{Ox}(\vec{r},t)\rangle_{V_R} \tag{13}$$

Within the range of validity of the zero-order reaction rate the former equation can be immediately integrated, with just the initial condition: $C_{Ox}(t=0) = C^0_{Ox}$, to yield *initial* rate data:

$$\left\langle R^0_{Ox}(\vec{r})\right\rangle_{V_R} = -\frac{V^{II}_T}{V_R}\left(\frac{C_{Ox}(t) - C^0_{Ox}}{t - t_o}\right) \tag{14}$$

Table 3 details the experimental conditions, together with actinometry (output power) and initial reaction rates of decomposition of the oxalic acid solution for a representative set of experimental runs.

It is now necessary to consider how to compare, adequately, the performances of the immobilized versus the slurried photocatalyst. Then, an apparent quantum efficiency of the decomposition of oxalic can be defined, as follows:

$$\eta_{V_R} = \frac{\left\langle R^0_{Ox}(\vec{r})\right\rangle_{V_R}}{(P_C/V_R)} \times 100 \tag{15}$$

where the reactor volume, V_R, represents either the fluidized bed volume or the full annular space, according to the case. Also, for comparison purposes, it is appropriate to consider the *specific* initial reaction rate (i.e., per unit mass of titania inside the device)

Table 3
Experimental conditions employed in the photocatalytic decomposition of oxalic acid

Reacting system	Bed expansion	Surface coverage (nominal)	Output power[a,b]	Initial reaction rate	
			Einstein $s^{-1} \times 10^6$	$\langle R^0_{Ox}\rangle_{V_R}$	$\langle R^0_{Ox}\rangle_{V_{Liq}}$
				mol s^{-1} $cm^{-3} \times 10^{12}$	mol s^{-1} $cm^{-3} \times 10^{12}$
Suspension	–	–	0.90	163.8	163.8
FB[c]	7.0	0	1.83	–	–
FB[c]	7.0	30	1.51	24.6	28.5
FB[c]	7.0	60	1.28	26.1	32.2
FB[c]	7.0	100	1.11	27.8	32.2
FB[c]	3.8	0	1.04	–	
FB[c]	3.8	30	0.69	21.0	28.6
FB[c]	3.8	60	0.45	25.2	34.3
FB[c]	2.3	0	0.24	–	–
FB[c]	2.3	30	0.12	19.1	33.8

[a] The incident power onto the inner surface of the reaction space (P_{IN}) was equal to 4.34310^{-6} Einstein s^{-1}.
[b] The output power from the masked reactor (P_M) was equal to 0.097310^{-6} Einstein s^{-1}.
[c] Fluidized bed.

$$\left\langle R^0_{Ox}(\vec{r})\right\rangle^{TiO_2}_{V_R} = \frac{\langle R^0_{Ox}(\vec{r})\rangle_{V_R}}{\left[C_{TiO_2}\right]_{V_R}} \quad (16)$$

and, accordingly, to define a *specific* apparent quantum efficiency of the photocatalytic decomposition:

$$\eta^{TiO_2}_{V_R} = \frac{\eta_{V_R}}{\left[C_{TiO_2}\right]_{V_R}} \quad (17)$$

Fig. 8 presents, in matrix format, the initial reaction rates and apparent quantum efficiencies, together with their corresponding specific values, as a function of bed expansion and per cent of surface coverage. The equivalent parameters for the free titania suspension are also included in the diagram. [1]

At first sight it can be observed that the rate of reaction and the apparent quantum efficiency for the free suspension of titania is about 5–6 times higher that those obtained with the immobilized catalyst in the fluidized beds. Several factors may contribute to this lower performance of the anchored catalyst: reduction of available surface area resulting from the binding with the supporting surface of the quartz sand, significant radiation extinction (absorption and scattering) by the support, or catalyst agglomeration (surface clumping) during fixation, among others. Also, even though for an adequate fluidized bed operation, mass transfer limitations should not be present, one can not entirely disregard this possible effect.

Focusing on the fluidized bed results, it comes out that the reaction rate and also the apparent quantum efficiency are fairly sensitive to bed expansion and surface coverage. A total increment of almost 50% in reaction rate and of nearly 100% in ν_{VR} results by using more expanded fluidized beds with well covered quartz sand, while keeping the concentration of photocatalyst inside the reaction vessel as the constant parameter (250 ppm; matrix diagonal). At a given surface coverage (e.g., the first column in the figure) the increments in reaction rate and quantum efficiency are somewhat lower but still significant (31 and 95%, respectively). This is remarkable, considering that the concentration of photocatalyst, $\left[C_{TiO_2}\right]_{V_R}$ is lower than the higher the expansion of the fluidized bed is. However, for any given bed expansion the increment in reaction rate is just mild and the apparent quantum efficiency is rather insensitive to the surface coverage. This finding, incidentally, shows that the detrimental effects of attrition on the surface coating may not actually damage a photocatalytic abatement process beyond hope. In other words, a well-covered support may perform well even

[1]

$$\left\langle R^0_{Ox}\right\rangle_{V_R} [=] \begin{array}{l}[(\text{moles oxalic acid reacted} @\, t=0)/ \\ (\text{cm}^3 \text{ reactor volume})\ (\text{s})] \times 10^{12}\end{array}$$

$$\left\langle R^0_{Ox}\right\rangle^{TiO_2}_{V_{Liq}} [=] \frac{\begin{array}{c}(\text{moles oxalic acid reacted} @\, t=0)\,/ \\ (\text{cm}^3 \text{ liquid reactor volume})\ (\text{s})\end{array}}{(\text{grams } TiO_2)\,/\,(\text{cm}^3 \text{ reactor volume})} \times 10^9$$

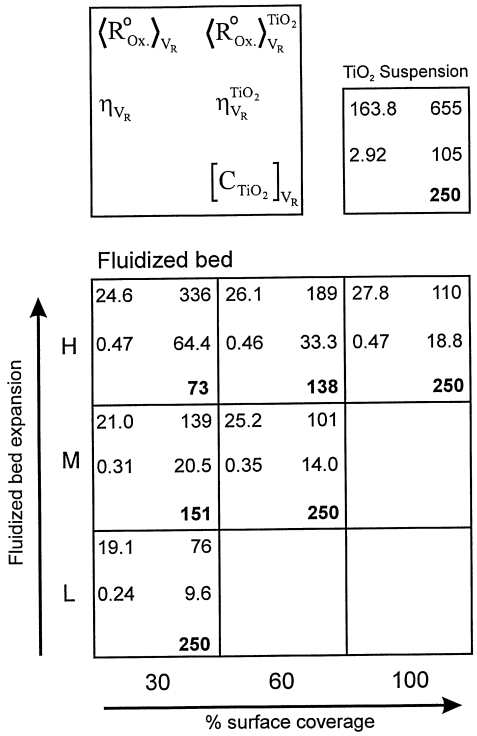

Fig. 8. Initial reaction rate and apparent quantum efficiency of the decomposition of oxalic acid (first column in each box) and specific initial reaction rate and apparent quantum efficiency of the decomposition of oxalic acid, per unit mass of photocatalyst inside the reactor space (second column in each box) for the TiO_2 used in suspension (250 ppm) or in fluidized bed form, for different bed expansions and percentages of surface coverage of the quartz sand [see Eqs. (14)–(17). For reference purposes the concentration of photocatalyst inside the reaction space is also included in the diagram (lower right corner of each box, boldface).

though the surface coating may get reduced down to a 30% of the initial surface coverage.

Regardless, this low sensitivity to the rising of surface coverage may indicate that an increase in the catalyst loading could be actually producing an increase in the agglomeration of the catalyst elementary particles during immobilization rather than an augmentation of the available catalyst active surface area.

As for the *specific* reaction rate and apparent quantum efficiencies, again the suspension is both more active and more efficient than any of the fluidized beds, but just twice as good if a highly expanded bed with 30% surface coverage is used. This result is quite relevant, because it indicates that advanced photocatalysts (probably more expensive than the titania pigments now under scrutiny) can be advantageously fixed onto suitable supports and employed in fluidized bed reactors.

Going back to the fluidized beds, it is apparent that the specific rates and/or quantum efficiencies achieved with highly expanded beds containing just moderate coverage of photocatalyst are noticeably higher than those attainable under any other process condition.

Yet, in fluidized beds the volume fraction of solid is never negligible. The volume of liquid phase that can be processed inside the photocatalytic reactor is lower the lower the bed expansion is. This constraint led us to consider decomposition rates and apparent quantum efficiencies referred to the actual liquid volume rather than the total volume of the reactor, entirely equivalent to Eqs. (14)–(17) defined above:

$$\left\langle R^0_{Ox}(\vec{r})\right\rangle_{V_{Liq}} = -\frac{V^{II}_T}{V_{Liq}}\left(\frac{C_{Ox}(t) - C^0_{Ox}}{t - t_o}\right) \tag{18}$$

$$\eta_{V_{Liq}} = \frac{\left\langle R^0_{Ox}(\vec{r})\right\rangle_{V_{Liq}}}{(P_C/V_R)} \times 100 \tag{19}$$

$$\left\langle R^0_{Ox}(\vec{r})\right\rangle^{TiO_2}_{V_{Liq}} = \frac{\left\langle R^0_{Ox}(\vec{r})\right\rangle_{V_{Liq}}}{[C_{TiO_2}]_{V_R}} \tag{20}$$

$$\eta^{TiO_2}_{V_{Liq}} = \frac{\eta_{V_{Liq}}}{[C_{TiO_2}]_{V_R}} \tag{21}$$

Fig. 9 shows, again in matrix format, absolute and specific values of rates of reaction and of apparent quantum efficiencies as a function of bed expansion and per cent of surface coverage. They are referred now to the net liquid volume (V_{Liq}) in the reacting space. Once more, the corresponding parameters for the free titania suspension are included in the diagram. [2]

Certainly, under this new point of view, both the rate of reaction and the apparent quantum efficiency

[2]

$\left\langle R^0_{Ox}\right\rangle_{V_{Liq}}$ [=] [(moles oxalic acid reacted @ $t = 0$)/ cm^3 liquid reaction volume (s)] $\times 10^{12}$

$$\left\langle R^0_{Ox}\right\rangle^{TiO_2}_{V_{Liq}}\ [=]\ \left[\frac{\text{(moles oxalic acid reacted @ } t = 0)/\text{ (cm}^3\text{ liquid reaction volume) (s)}}{\text{(grams TiO}_2)/(\text{cm}^3\text{ reactor volume)}} \times 10^9\right]$$

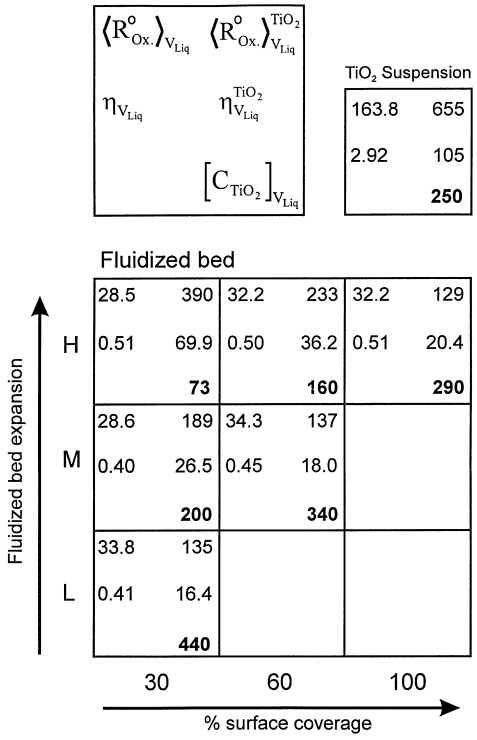

Fig. 9. Initial reaction rate and apparent quantum efficiency of the decomposition of oxalic acid (first column in each box) and specific initial reaction rate and apparent quantum efficiency of the decomposition of oxalic acid, per unit mass of photocatalyst inside the reactor space (second column in each box:), for the TiO_2 used in suspension (250 ppm) or in fluidized bed form, for different bed expansions and percentages of surface coverage of the quartz sand [see Eqs. (18)–(21)], per unit volume of liquid phase. For reference purposes the concentration of photocatalyst inside the reaction space per unit volume of liquid phase is also included in the diagram (lower right corner of each box, boldface).

for the free suspension of titania are also about 5–6 times higher that those obtained with the immobilized catalyst in the fluidized beds. Among the fluidized beds, though, it comes out that the reaction rate and the apparent quantum efficiency become less sensitive to bed expansion or surface coverage. The increment in reaction rate is negligible and the apparent quantum efficiency only increases by 24% when the more expanded fluidized bed with well-covered quartz sand is used, and the concentration of photocatalyst inside the reaction vessel is kept constant (matrix diagonal). At a given surface coverage (e.g., the first column in the diagram) the reaction rate actually decreases the higher the expansion of the bed is made, albeit mildly (15%). Altogether, these data indicate that, if catalyst cost is not a constraint, the reaction rate and/or the apparent quantum efficiencies for about any combination of fluidized bed expansion and surface coverage, referred to the net liquid volume, are rather similar in all cases.

In order not to mislead the reader it has to be recalled that all of our data were obtained with the same photoreactor (i.e., the same radial gap was always employed). So, because a highly expanded bed of moderately covered support particles captures less radiation power (see Fig. 7), under these process design conditions a FIP operation can be sustained in an annular photoreactor with a larger gap and, hence, larger volumes of polluted solutions could be processed with the same radiation source.

5. Conclusions

For the same starting material (Degussa P-25) and with the same catalyst loading inside a fully illuminated photoreactor, the supported titania operating in fluidized beds shows a significant decrease in photocatalytic conversion and apparent quantum efficiency as for destroying a model reactant (oxalic acid) in comparison with the performance achieved using the photocatalyst as a slurry of the free powder.

Having used the same catalyst and employed a suitable, low calcination temperature during the fixation process, it is not yet clear why the supported catalyst undergoes such a significant loss of chemical activity upon fixation.

The immobilized catalyst, though, does not require downstream solid–liquid separations. So, if owing to separation costs the immobilized catalyst is necessary, the highly expanded fluidized bed seems to be the best option: it provides the best performance and, at the same time, it allows the use of a larger reactor optical path (i.e., a larger reactor volume for the same lamp), which signifies that larger throughputs can be realized using these type of ‘optically thin’ fluidized beds.

6. Nomenclature

A area, cm^2
C concentration, $mol\,cm^{-3}$, also mM, also ppm

e^a	local volumetric rate of energy absorption (LVREA), Einstein $cm^{-3}\,s^{-1}$
G	incident radiation, Einstein $cm^{-2}\,s$
I	specific intensity, Einstein $cm^{-2}\,s^{-1}\,sr$
L	length, cm
P	radiant power, W, also Einstein s^{-1}
R	reaction rate, mol $cm^{-3}\,s^{-1}$
$\vec{r}$	position vector, cm
r	radius, cm
t	time, s
V	volume, cm^3
z	cylindrical co-ordinate, cm

7. Greek letters

α	cylindrical co-ordinate, rad
η	apparent quantum efficiency, mol $Einstein^{-1}$
θ	spherical co-ordinate, rad
λ	wavelength, nm
ϕ	volumetric fraction, dimensionless
φ	spherical co-ordinate, rad
Ψ	partitional factor, defined by Eq. (12), dimensionless
Ω	solid angle, sr
$\vec{\Omega}$	unit vector in the direction of propagation, dimensionless

8. Subscripts

Act	relative to the actinometer
C	indicates captured power
CS	indicates coated sand
e	relative to an external radius
Fe^{2+}	relative to ferrous ion
FB	relative to the fluidized bed
i	relative to an internal radius
IN	indicates incoming radiation
Liq	relative to liquid phase
L	relative to the lamp
M	relative to 'masked' reactor
Ox	relative to oxalic acid
OUT	indicates ' out going' radiation
R	relative to reactor volume
TiO_2	relative to the photocatalyst
T	relative to the reservoir in a reaction loop
s	relative to solid phase
Susp	relative to titania suspension
V	relative to volume
λ	relative to wave length dependence
w	relative to the reactor wall

9. Superscripts

Act	relative to the actinometer
FB	relative to fluidized bed
0	relative to initial conditions
Ox	relative to oxalic acid
TiO_2	relative to the photocatalyst

10. Special symbols

$\rightarrow$	indicates a vectorial quantity
$\langle\rangle$	indicates an average value
$\vert_x$	indicates an integration point

Acknowledgements

Thanks are given to José L. Giombi for his skilled technical assistance. The financial support of Universidad Nacional del Litoral (UNL), Consejo Nacional de Investigaciones Científicas y Técnicas (CONICET) and Programa de Modernización Tecnológica, PID 022 (ANPCyT) is gratefully acknowledged.

Appendix A

In the most general case, radiation may be arriving at one point inside a photochemical reactor from all directions, $\vec{\Omega}$, in space. Hence, for a polychromatic lamp and a diactinic non participating medium, the incident radiation onto a point located at any arbitrary position $\vec{r}$ with respect to a fixed coordinate system can be expressed as:

$$G(\vec{r}) = \int_{\lambda}\int_{\Omega} I_{L,\lambda}\left(\vec{r}, \vec{\Omega}\right) d\Omega\, d\lambda \qquad (A.1)$$

where $I_{L,\lambda}$ is the spectral intensity emitted by the emission source.

Eq. (A.1) can be easily transformed to give an expression for the incident radiation impinging onto a point located at the internal wall of our annular reaction system, $G_{w_{r_i}}$, upcoming from its axially centered lamp, in terms of Einstein $s^{-1}\,cm^{-2}$. So, by using spherical coordinates and considering the lamp as a three dimensional source with superficial diffuse emission, the following equation can be written:

$$G_{w_{r_i}} = \int_{\lambda}\int_{\varphi_1}^{\varphi_2}\int_{\theta_1}^{\theta_2} I_{L,\lambda}\,(\vec{r})|_{r=r_i} \sin\theta\, d\varphi\, d\theta\, d\lambda \quad (A.2)$$

Here, the system of coordinates is located at the incidence point and the integration limits: (φ_1,φ_2) and (θ_1,θ_2) can be found straightforwardly, as trigonometric functions of the system geometry. They correspond to the solid angle determined by the lamp boundaries, as seen from the position of the point of incidence (for more details see [16]).

From Eq. (A.2) the incident radiation power onto any portion of the internal surface of the reactor wall can be readily be computed by:

$$P_{w_{r_i}} = \int_{A_{r_i}} G_{w_{r_i}}\, dA_{r_i} \quad (A.3)$$

However, given the cylindrical symmetry of the reactor surface, it is obviously more convenient to use cylindrical coordinates: (r, α, z). Therefore, at $r = r_i$:

$$P_{w_{r_i}} = \int_{\alpha}\int_{z} G_{w_{r_i}}\,(z,\alpha)\, r_i\, dz\, d\alpha \quad (A.4)$$

which, given the azimutal symmetry of the photoreactor can be reduced, for any cylindrical portion, to [16]:

$$P_{w_{r_i}} = 2\pi r_i \int_{z} G_{w_{r_i}}\,(z)\, dz \quad (A.5)$$

By integrating on z between any pairs of reactor lengths, the incident power onto that portion of the inner surface of the reactor (defined by these limits) can be determined. In particular, this can be done for the suspended bed and the fluidized bed lengths, respectively. Hence, a partition factor Ψ_{FB} between these two types of operation of the reactor results:

$$\Psi_{FB} = \frac{\int_{z=0}^{z=z_{FB}} G_{w_{r_i}}\,(z)\, dz}{\int_{z=0}^{z=z_{Susp}} G_{w_{r_i}}\,(z)\, dz} \quad (A.6)$$

For the geometrical configuration of our system $\Psi_{FB} = 0.98$.

References

[1] D. Ollis, H. Al-Ekabi, Photocatalytic Purification and Treatment of Water and Air, Elsevier, Amsterdam, 1993.
[2] A.L. Linsebigler, Guangquan Lu, J.T. Jates Jr, Chem. Rev. 95 (1995) 735.
[3] D. Ollis, E. Pellizzetti, N. Serpone, Environ. Sci. Technol. 25 (1991) 1523.
[4] M.R. Hoffmann, M.T. Martin, W. Choi, D.W. Bahnemann, Chem. Rev. 95 (1995) 69.
[5] C.S. Turchi, D.F. Ollis, J. Catal. 122 (1990) 178.
[6] N. Peill, M. Hoffmann, Environ. Sci. Technol. 30 (1996) 2806.
[7] R. L Pozzo, M.A. Baltanás, A.E. Cassano, Catal. Today 39 (1997) 210.
[8] J.M. Herrmann, M.N. Mozzanega, P. Pichat, J. Photochem. 22 (1983) 333.
[9] M. Litter, J.A. Navío, J. Photochem. Photobiol. A: Chem. 84 (1994) 183.
[10] C.A. Martin, M.A. Baltanás, A.E. Cassano, J. Photochem. Photobiol. A: Chem. 94 (1996) 173.
[11] G. Spadoni, E. Bandini, F. Santarelli, Chem. Eng. Sci. 33 (1978) 517.
[12] C. Stramigioli, G. Spadoni, F. Santarelli, Int. J. Heat Mass Transfer 21 (1978) 660.
[13] M.I. Cabrera, O.M. Alfano, A.E. Cassano, J. Phys. Chem. 100 (1996) 20043.
[14] N.B. Jackson, C.M. Wang, Z. Luu, J. Schwitzgebel, J.G. Ekerdt, J.R. Brock, A. Heller, J. Electrochem. Soc. 138(12) (1991) 3660.
[15] S.L. Murov, J. Carmichael, G.L. Hug, Handbook of Photochemistry, 2 edn., M. Dekker, New York, 1993.
[16] A.E. Cassano, C.A. Martin, R.J. Brandi, O.M. Alfano, Ind. Eng. Chem. Res. 34 (1995) 2155.